IEEE Access
Multidisciplinary | Rapid Review | Open Access Journal

Received 4 April 2023, accepted 12 April 2023, date of publication 18 April 2023, date of current version 24 April 2023.

Digital Object Identifier 10.1109/ACCESS.2023.3268033

RESEARCH ARTICLE

Investigation of n-ZnO/p-Si and n-TiO_2/p-Si Heterojunction Solar Cells: TCAD + DFT

JASURBEK GULOMOV[1], OUSSAMA ACCOUCHE[2], (Associate Member, IEEE), RAYIMJON ALIEV[1], RAYMOND GHANDOUR[2], (Senior Member, IEEE), AND IRODAKHON GULOMOVA[1]

[1]Renewable Energy Sources Laboratory, Andijan State University, Andijan 170100, Uzbeksitan
[2]College of Engineering and Technology, American University of the Middle East, Egaila 54200, Kuwait

Corresponding author: Jasurbek Gulomov (jasurbekgulomov@yahoo.com)

ABSTRACT This paper focuses on exploring new materials and structure as a means to increase the efficiency of solar cells. Since silicon is widespread on earth, it is desirable to study heterojunction solar cells made mainly of silicon and new materials. Therefore, ZnO/Si and TiO_2/Si heterojunction solar cells were studied in this paper. First, the electrical and optical properties of ZnO and TiO_2 were determined using the Perdew-Burke-Ernzerhof (PBE), PBE functional revised for solids (PBESol) and Perdew-Wang (PW91) functionals of the Generalized gradient approximation (GGA) in Density Functional Theory (DFT). The obtained results in various functionals are assessed and analyzed. It was found that geometric optimized structures of TiO_2 and ZnO is mechanical stable. Accordingly, in all functionals, the effective mass of the electron in ZnO and TiO_2 proved to be smaller than that of the hole. The mobility of electrons and holes in ZnO was calculated to be 430.72 $cm^2V^{-1}s^{-1}$ and 5.25 $cm^2V^{-1}s^{-1}$ respectively. In TiO_2, it was 355.27 $cm^2V^{-1}s^{-1}$ and 46.38 $cm^2V^{-1}s^{-1}$. When PW91, PBESol, PBE functionals were used, the dielectric constant was determined to be 11, 11.5, 8.5 for ZnO and 9.5, 10, 9 for TiO_2, respectively. According to the DFT results, it was determined that ZnO and TiO_2 are transparent and mainly n-type direct semiconductors. According to device simulation, the maximum short-circuit current of ZnO/Si and TiO_2/Si heterojunction solar cells is 18 mA/cm^2 at a thickness of 80 nm and 15.3 mA/cm^2 at a thickness of 40 nm. Finally, the average fill factor of ZnO/Si and TiO_2/Si solar cells was 0.73 and 0.76 respectively. So TiO_2 can be used as a transparent contact and ZnO as an emitter layer in a silicon-based solar cell.

INDEX TERMS Numerical simulation, heterojunctions, silicon, density functional theory, titanium dioxide, zinc oxide.

I. INTRODUCTION

Solar cells are a promising solution to meet the growing demand for electricity as the world's demand for electric energy continues to increase and natural resources become scarce. However, their high cost and low efficiency have been the main reasons for their slow adoption. In industry, solar cells are mainly made out of silicon. The maximum efficiency of silicon-based homojunction solar cells can reach 29% in theory [1]. However, in the experiment, it is around 24% [2]. This difference is due to thermal, optical and electrical losses [3]. To overcome optical losses, an anti-reflection layer [4] is coated on the surface of the solar cell and various textures [5] are created. Due to spectral characteristics mismatch [6], silicon mainly absorbs light in the visible range [7] and does not absorb ultraviolet or infrared. To address the issue of the spectral mismatch and to enhance optical absorption, the surface of solar cells is coated with luminescent materials [8]. Additionally, metal nanoparticles [9] and quantum dots [10] are also incorporated into the solar cell to increase the optical absorption. In our previous scientific work, the effect of gold, silver, platinum and copper nanoparticles on a silicon-based solar cell was examined [11]. Consequently, gold nanoparticles have a great effect on silicon heterojunction solar cells [12]. When high-energy photons are absorbed in silicon, high-energy electrons

The associate editor coordinating the review of this manuscript and approving it for publication was Chong Leong Gan.

are generated [13]. These electrons quickly recombine and lose energy. The generated energy is then transferred to the crystal lattice and leads to heating [14]. Down-shifting luminescent materials absorb high-energy photons and emit low-energy photons [15]. Therefore, by coating the solar cell with down-shifting luminescent materials [16], it is possible to reduce the spectral mismatch and prevent the heating of the crystal lattice. Since silicon-based solar cells do not absorb infrared rays. They are absorbed at the back contacts. Metals heat up when they absorb infrared light [17]. Therefore, to prevent the solar cell from overheating, the back contact should be in the form of a grid, not solid [18]. To minimize the surface recombination of high-energy electrons in silicon-based solar cells, the surface is treated with SiO_2 [19] and SiN_x [20] coatings, which helps to reduce the high recombination rate caused by the incomplete bonds on the material's surface.

The theoretical efficiency limit of a solar cell is the maximum efficiency that can be achieved by a solar cell based on its material properties and design. By studying the surface morphology, geometric dimensions, anti-reflective layers and contact types of a solar cell, it is impossible to overcome this limit. Therefore, it is necessary to find new materials for solar cells. Over the past decade, there has been a huge interest in perovskite [21], organic materials [22] and metal oxides [23] as potential candidates for solar cells. Accordingly, the efficiency of perovskite-based solar cells has seen a significant improvement from 3.9% to 25.5% [24]. Similarly, organic solar cells have reached a maximum efficiency of 19% [25]. Metal oxides mainly act as a layer that conducts charge carriers in casterite, perovskite and organic solar cells [26]. Because the electron affinity, the mobility of charge carriers, band gap, the type of electrical conductivity of metal oxides is used as electron transport (ETL) [27] or hole transport layer (HTL) [28]. Metal oxides can be n-type or p-type conductivity during synthesis. For example, in the process of synthesis, ZnO is n-type [29], and NiO_x is p-type [30]. Metal oxides can be used to make transparent solar cells for windows [31]. The n-ZnO/p-NiO_x heterojunction solar cell is transparent and its maximum efficiency is 6% [32].

Even though homojunction solar cells have been optimized, their efficiency cannot exceed the Shockley-Quisser limit. For this reason, designing 2-junctions, 3-junctions and multijunction solar cells is considered more effective [33]. Tandem solar cells have a higher efficiency due to their ability to absorb a wider spectrum of light. In an experiment, a GaAs-based multijunction solar cell showed the highest efficiency among its peers, reaching 47.1% [34]. Theoretically, an infinite number of multijunction solar cells can achieve a maximum efficiency of 86.8% [35]. Since silicon is the most common material on earth, it is appropriate to use solar cells based on it. A technology for the industrial production of a silicon/perovskite tandem solar cell with an efficiency of 28.7% has been developed [36]. Besides, heterojunction solar cells can overcome theoretical efficiency of solar cell [37].

Metal oxides can be used as front contacts for silicon-based solar cells because they are transparent and have good electrical conductivity. This transparent contact helps to reduce the shadow effect on the solar cell [38]. Additionally, metal oxides can act as an anti-reflection layer for a silicon-based solar cell due to their optimal refractive index. As mentioned before, metal oxides can be used as ETL or HTL. Metal oxides can also be used to form an emitter layer on the surface of a silicon-based solar cell. Hence, it is possible to create a heterojunction solar cell with a high efficiency by depositing an n-type metal oxide on the p-type silicon surface. This paper examines the optical and electronic properties of TiO_2 and ZnO throughout detailed analysis using DFT. ZnO/Si and TiO_2/Si heterojunction solar cells were simulated using TCAD and analyzed in depth. For device simulation, material properties are very important to get good results. ZnO and TiO_2 are well researched materials in computational [39] and experimental [40] material sciences. Besides, ZnO and TiO_2 based solar cells [41] also well studied. Mainly, in research article, author focus on device or material. In our article, we focus on both of device and materials. In device simulation, materials properties are taken from articles and other reliable sources. But we determined necessary properties of ZnO and TiO_2 for device simulation using DFT instead of getting them other researcher's works. Because, obtained results in devices simulation can be detailed analyzed and proved scientifically using DFT results. So, another difference is we tried to build atom to device simulation chain to study TiO_2/ZnO/Si heterojunction solar cells. Besides, TiO_2 and ZnO are usually used as antireflection coating [42] in silicon solar cell not emitter layer. TiO_2 and ZnO are not new material for solar cell. But, application of TiO_2 and ZnO such as emitter layer, finding optimal thickness of emitter layer, differentiate which material more suitable to be emitter or contact and different approach to research are novelty of this article.

In the next section, materials and used methods will be discussed in details.

II. MATERIALS AND METHODS

In this paper, DFT (Density functional theory) [43] method is used to calculate the electronic and optical properties of metal oxides. Sentaurus TCAD software was used to determine the photoelectric parameters of metal oxide/silicon heterojunction solar cells. The ZnO and TiO_2 parameter files are not available in the Sentaurus TCAD material database. To model devices based on materials that are not available in the database, parameter files containing the necessary physical properties of these materials are created using information from the literature. However, the desired physical properties of the material can be calculated using DFT. In this scientific work, we calculated the necessary physical properties of ZnO and TiO_2 using the Cambridge Serial Total Energy Package (CASTEP) code. This combined approach of DFT and TCAD allowed for the creation of a

modeling chain that extended from the atomic level to the device level.

A. COMPUTATION OF MATERIAL PROPERTIES

Calculation of the physical properties of metal oxides based on DFT was performed with the on-the-fly generation (OTFG) ultrasoft pseudopotential using the CASTEP code. Exchange-correlation interactions were calculated using Generalized gradient approximation (GGA) Perdew-Burke-Ernzerhof (PBE) [44], PBE functional revised for solids (PBEsol) [45] and Perdew-Wang (PW91) [46] functionals. The calculation was carried out in two stages: Geometric optimization and energy calculation. In order to calculate an arbitrary parameter of the material, such as elastic, electronic, or optical, it is first necessary to perform geometric optimization to stabilize the structure. The Broyden–Fletcher–Goldfarb–Shanno (BFGS) [47] algorithm was used to find the lowest energy configuration between the atoms of the crystal lattice. In the geometric optimization, the convergence criteria for energy, force, stress, and displacement are 2E-5 eV/atom, 0.05 eV/A, 0.1 GPa, and 0.002 A, respectively. $5 \times 5 \times 4$ Monkhorst-Pack [48] grids of k-points for ZnO and $3 \times 3 \times 5$ for TiO_2 as a Brillouin zone pattern of the crystal structure are adapted to determine the zone diagram and optical properties. The convergence criteria of kinetic energy limit, total energy and residual force relaxation were taken as 571.4 eV, 1E-6 eV/Atom and 0.07 eV/A, respectively.

B. DEVICE SIMULATION

Four instruments of Sentaurus TCAD were utilized in the modeling of the device: Sentaurus Structure Editor, Sentaurus Device, Sentaurus Visual, Sentaurus Workbench. A geometric model of the solar cell was developed using the Sentaurus Structure Editor, in which the size, material, type and concentration of the doped atom of each region were specified [49]. In addition, since the calculation was carried out using a numerical method, the device was meshed with the required dimensions [50]. The geometric model created in the Sentaurus Structure Editor was then transferred to the Sentaurus Device. In Sentaurus Device, firstly, the required physical properties of materials were assigned. If the material of the device is available in the Sentaurus TCAD material database, its physical parameters are taken from the database. For materials that do not exist in the material database, a new parameter file is created or its physical parameters are written directly as a function in the command file. It is preferable to create a new parameter file for a new material. Because it can be included in the material base of Sentarus TCAD and used in further work. The necessary physical parameters of new materials are mainly found in the literature. However, in this scientific work, the physical parameters of ZnO and TiO_2, which were not available in the Sentaurus TCAD database, were calculated using DFT and used in the modeling. After the necessary physical parameters of each material were provided, calculations were made using physical models and mathematical operators to determine the physical characteristics of the device. In the next sub-section, the theoretical basis of the numerical simulation of the solar cell is explained in details.

C. THEORY OF DEVICE SIMULATION

In modeling semiconductor devices, the internal electric field, potential, and transport of charge carriers are important. To model a simple diode in equilibrium, it is enough to determine electric field and potential using Poisson's equation given by equation 1 [51].

$$\Delta\varphi = -\frac{q}{\varepsilon}(p - n + N_D + N_A) \tag{1}$$

where: ε is the permittivity, n and p are the electron and hole concentrations, respectively, N_D and N_A are the concentrations of donor and acceptor, respectively, and q is the charge.

Because electrons belong to the family of fermions, the concentration of charge carriers in the Poisson equation is calculated using the Fermi function presented in equation 2 [52].

$$\begin{aligned} n &= N_c F_{1/2}\left(\frac{E_{F,n} - E_c}{kT}\right) \\ p &= N_V F_{1/2}\left(\frac{E_V - E_{F,p}}{kT}\right) \end{aligned} \tag{2}$$

where: N_c and N_v are the densities of the states in the conduction and the valence bands, respectively, E_c is the minimum energy of the conduction band, E_v is the maximum energy of the valence band, T is the temperature, k is the Boltzmann constant, and $E_{F,n}$ and $E_{F,p}$ are the quasi-fermi energies.

The movement of charge carriers in a diode is driven by the internal electric field. The transport of charge carriers is calculated using the drift-diffusion model of continuity. The drift-diffusion model calculates the current formed due to the difference in the concentration of charge carriers and the electric field. It is presented in equation 3 [53]

$$\begin{aligned} J_n &= -nq\mu_n \nabla\Phi_n \\ J_p &= -pq\mu_p \nabla\Phi_p \end{aligned} \tag{3}$$

where: J_n and J_p are electron and hole currents, respectively, μ_n and μ_p are electron and hole mobilities, respectively, and Φ_n and Φ_p are the electron and hole quasi-Fermi potentials.

The composition of the solar cell consists of a p-n junction, like a diode. Only, when modeling the solar cell, it is necessary to take into account the effect of light. Ray Tracing [54], Transfer Matrix Method (TMM) [55] and Beam Propogation [56] methods are widely used for optical modeling of solar cells. In this paper, the optical modeling was performed using the TMM method. Because, in TMM, the internal interference formed in the layers of the solar cell and the surface roughness are also taken into account. The Fresnel equations (equation 4) were used as optical boundary

conditions.

$$\begin{cases} r_t = \dfrac{n_1 \cos\beta - n_2 \cos\gamma}{n_1 \cos\beta + n_2 \cos\gamma} \\ t_t = \dfrac{2n_1 \cos\beta}{n_1 \cos\beta + n_2 \cos\gamma} \end{cases} \quad and \quad \times \begin{cases} r_p = \dfrac{n_1 \cos\gamma - n_2 \cos\beta}{n_1 \cos\gamma + n_2 \cos\beta} \\ t_p = \dfrac{2n_1 \cos\beta}{n_2 \cos\beta + n_1 \cos\gamma} \end{cases} \tag{4}$$

where: r_t and t_t are the Fresnel coefficients for transversal polarized light, r_p and t_p are the Fresnel coefficients for parallel polarized light, n_1 and n_2 are the refractive indices of first and second media, β is the angle of the incident light, and γ is the angle of refracted light.

The photogeneration in the solar cell is calculated by the quantum yield function [57]. It is a logical function. If the photon energy falling on the solar element is greater than the band gap of material, it is absorbed, and hence the logic function is equal to 1, otherwise it is 0. Electron-hole pairs generated in the solar cell are separated due to the internal electric field and are directed to the contacts (metal plates) at the edges of the cell. However, when the charge carriers move through the semiconductor, they recombine, and thus some of the generated charge carriers can no longer reach the contacts. Since TiO_2 and ZnO are direct semiconductors, radiative, Auger and Shockley-Read-Hall (SRH) recombination were calculated. In the silicon region, only Auger and SRH recombinations were calculated. Because silicon is an indirect semiconductor, the percentage of radiative recombination is almost less than 1%. The current and potential generated in the contacts are determined by the electrical boundary conditions given in equation 5.

$$\begin{aligned} \varphi &= \varphi_F + \frac{kT}{q} \mathrm{a\,sinh}\left(\frac{N_D - N_A}{2n_{i,eff}}\right) \\ n_0 p_0 &= n_{i,eff}^2 \\ n_0 &= \sqrt{\frac{(N_D - N_A)^2}{4} + n_{i,eff}^2} + \frac{N_D - N_A}{2} \\ p_0 &= \sqrt{\frac{(N_D - N_A)^2}{4} + n_{i,eff}^2} - \frac{N_D - N_A}{2} \end{aligned} \tag{5}$$

where: $n_{i,eff}$ is the effective intrinsic carrier concentration, and φ_F is the Fermi potential of the contact.

The concentration, displacement, electric field and potential of charge carriers in solar cells are considered the same as in diodes.

III. RESULTS AND DISCUSSION

A. CRYSTAL STRUCTURE

It is important to create a correct and stable structure in the simulation of materials. First, the crystal structure of the materials is drawn. Then, the drawn structure is geometrically optimized to create a stable material and determine the optimal arrangement of atoms in the crystal lattice. In this work, ZnO and TiO_2 were geometrically optimized using PBE, PW91 and PBESol functionals. Figure 1 depicts the crystal structures of geometrically optimized ZnO and TiO_2 using the PBE functional. Table 1 highlights the dimensions of the crystal lattice for the geometrically optimized ZnO and TiO_2 structures obtained through the PBE, PW91, and PBESol functionals. ZnO has a hexagonal structure, its base consists of a parallelogram with equal sides and thus a and b parameters are equal to each other. On the other hand, TiO_2 has a PUC (primitive unit cell) tetragonal crystal structure, and its a and b parameters are mutually equal. Therefore, the crystal lattice of ZnO and TiO_2 is mainly characterized by parameters a and c. In the ideal case, the ratio of c and a depends on the type of material for the hexagonal structure (8/3)*0.5=1.633 [58] and PUC. In the experiment in [59], the crystal lattice constants of TiO_2 were determined to be a=4.6344 Å and c=2.9919 Å. In the experiment [60], the crystal lattice constants of ZnO were found to be a=3.2497 Å and c=5.206Å. According to the results given in table 1, the average error of lattice constants determined using PBE, PBESol, PW91 functionals when compared with experimental results was found to be equal to 0.012%, 2.5307%, 1.5702% in ZnO and 0.9856%, 0.73895%, 0.9471% in TiO_2, respectively. Hence, it was found that the crystal lattice constants calculated using PBESol for TiO_2 and PBE functional for ZnO are in close agreement with the experimental results.

TABLE 1. Crystal constants of geometrically optimized structures of ZnO and TiO_2 using PBE, PW91 and PBESol functionals.

		PW91	PBESol	PBE
ZnO	*a*, Å	3.323370	3.352239	3.249270
	b, Å	3.323370	3.352239	3.249270
	c, Å	5.251477	5.305232	5.205440
TiO_2	*a*, Å	4.713584	4.650330	4.594000
	b, Å	4.713584	4.650330	4.594000
	c, Å	2.986346	2.957963	2.959000

Total energy of structure should be minimum to be stable material. The conditions of mechanical stability of various crystals have been extensively studied by Felix [61]. By calculating the eigenvalues of the stiffness matrix, it is possible to determine the necessary and sufficient conditions for the elastic stability of hexagonal and tetragonal structures. The elements of the stiffness matrix of ZnO with hexagonal structure given in table 2 satisfied the conditions given in equation 6. ZnO consists of a mechanically stable hexagonal structure because elements of stiffness matrix satisfy equation 6.

$$\begin{aligned} &C_{11} > |C_{12}|, \quad 2C_{13}^2 < C_{33}(C_{11} + C_{12}), \\ &C_{44} > 0, \quad C_{66} > 0 \end{aligned} \tag{6}$$

where: C_{ij} are elements of stiffness matrix.

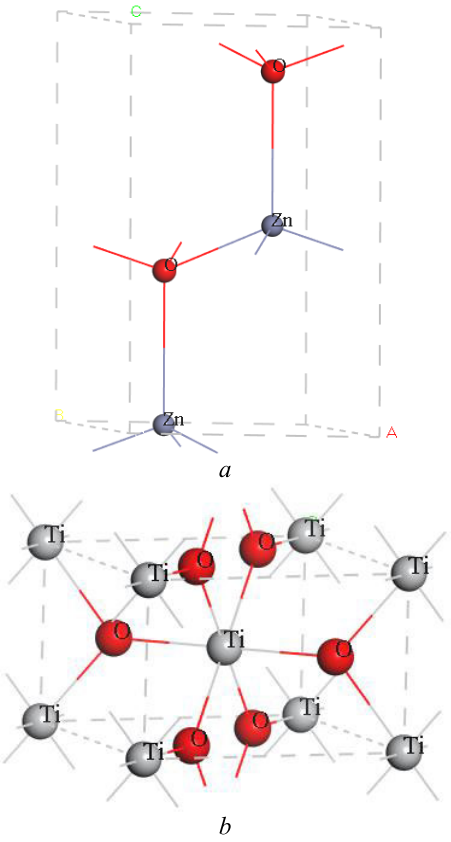

FIGURE 1. Crystal structure of ZnO (a) and TiO_2 (b).

TABLE 2. Elements of mechanical stiffness matrix of ZnO and TiO_2 calculated using PBE functional.

	ZnO	TiO_2
C_{11}, GPa	147.16890	299.19350
C_{12}, GPa	102.39525	149.66395
C_{13}, GPa	94.53912	145.93715
C_{16}, GPa		0.00000
C_{33}, GPa	202.51585	448.71985
C_{44}, GPa	39.44070	131.35465
C_{66}, GPa		214.05960

Since TiO_2 (P42/mnm) belongs to the (4/m) group of tetragonal structures, its mechanical stability cannot be determined using formula 6. Because, unlike other tetragonal structures, 4/m tetragonal structures have C_{16} and C_{66} elements in the stiffness matrix. Their mechanical stability is determined using the conditions given in equation 7. Since the stiffness matrix elements of TiO_2 given in table 2 satisfy the conditions in equation 7, it is proved that TiO_2 has a mechanically stable structure.

$$C_{11} > |C_{12}|, \quad 2C_{13}^2 < C_{33}\,(C_{11} + C_{12}),$$
$$C_{44} < 0, \quad 2C_{16}^2 < C_{66}\,(C_{11} - C_{12}) \tag{7}$$

B. BAND STRUCTURE

The electronic properties of the material are analyzed using a band structure. Figure 2 shows the calculated band structure

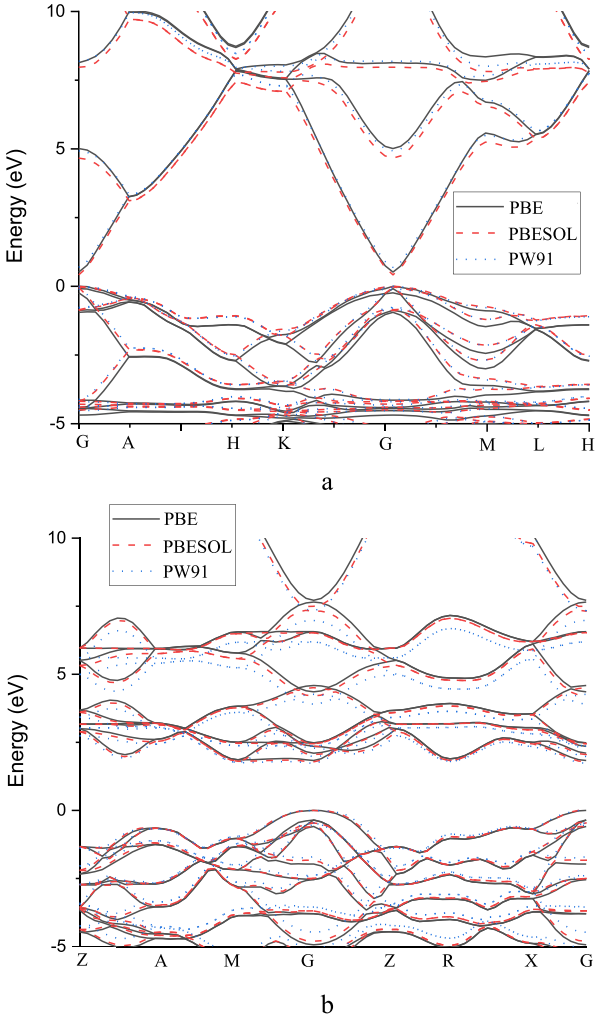

FIGURE 2. Band structure of ZnO(a) and TiO_2 (b) calculated using PBE, PBESol and PW91 functionals.

of ZnO and TiO_2 using different functionals. Quality of curves of band structures of TiO_2 and ZnO determined using the PBE, PW91, and PBESol functionals of GGA is almost similar. According to the results shown in figure 2, the minimum energy points of the conduction band and the maximum energy of the valence band of ZnO and TiO_2 correspond to the G. Therefore, both TiO_2 and ZnO are direct semiconductors.

When the band gap was determined from the band structure calculated using PBE, PBESol and PW91 functionals, it was found to be 0.518 eV, 0.415 eV, 0.688 eV for ZnO and 1.833 eV, 1.781 eV, 1.728 eV for TiO_2. In experiment, the band gap of ZnO and TiO_2 is 3.37 eV [62] and 3.2 eV [63], respectively. In calculating the band gap, PW91 functional achieved the best result among other functionals with 20.4% for ZnO and PBE with 57.3% accuracy for TiO_2. In Yuan's paper [64], PBESOL was found to be the most optimal functional for the calculation of metal oxides over other GGA functionals. Nevertheless, it is known that different metal oxides may require different functionalities, not only PBESol.

In our previous scientific work [65], it was found that the quality of curves of band structure of MoO_3 calculated using the HSE06 (Heyd-Scuseria-Ernzerhof) hybrid functional and the PBE functional is identical. Therefore, quality of curves of band structure calculated HSE06, GGA functionals and experiment may be the same. Hence, if the quality of the lines of the band structure is the same using different functions, their values can be adjusted by applying a fitting parameter. The fitting parameter is the ratio of the band structure determined in the experiment and in a function. For example, if the experimentally determined band gap of ZnO is 3.37 eV and the one calculated using PBE is 0.518 eV, then the fitting parameter for ZnO is equal to 6.5.

C. EFFECTIVE MASS

By analyzing the band structure of the material, some properties can be determined. One of these is the effective mass. In many materials, the lower points of the conduction region and the upper points of the valence region of the band structure obey the parabolic function given in equation 8.

$$E(k) = E_0 + \frac{\hbar^2 k^2}{2m^*} \tag{8}$$

where: E is the energy, E_0 is the energy at k = 0, k is the wavenumber, m^* is the effective mass, and $\hbar$ is the Planck constant.

To determine the effective masses of the electron and the hole, the E(k) band structure around the highest energy points of the valence band and the lowest energy of the conduction band is extracted from the band structure. Each E(k) is fit to a parabolic function using the least square method. Figure 3 shows the parabolic functions determined on the basis of E(k) band structure around the lowest energies of the conduction band and the highest energy of valence band of ZnO (a) and TiO_2 (b) calculated using PBE, PBESol, PW91 functionals.

The effective mass of the hole and electron was determined by differentiating the parabolic functions of the valence and conduction band twice with respect to k as given in equation 9:

$$m^* = \hbar^2 \left(\frac{d^2 E}{dk^2} \right) \tag{9}$$

Table 3 shows the hole and electron effective masses of ZnO and TiO_2 determined using PBE, PBESol and PW91 functionals. In experiment, the effective mass of electron and hole of ZnO is 0.24 and −0.59 [66]. The effective masses of electrons and holes of TiO_2 in the experiment are 0.5 [67] 4.66 [68]. The fact that the electron effective mass of ZnO and TiO_2 determined using all functionals is smaller than the effective mass of the hole satisfies the experimental results. According to table 3, the ratio of hole and electron effective masses determined in PW91, PBESol and PBE proves that the electron effective mass is smaller than the hole effective mass, which proves that ZnO and TiO_2 can be used as electron transport materials (ETM) in perovskite solar cells.

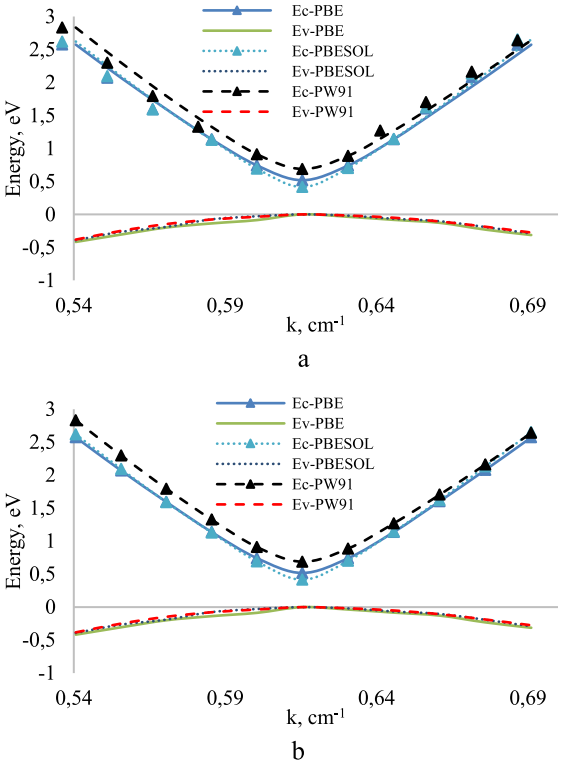

FIGURE 3. Parabolic approximations of the values around the minimum point of the conduction band and the maximum point of the valence band of ZnO (a) and TiO_2 (b).

TABLE 3. Effective masses of electron and hole in ZnO and TiO_2.

		PW91	PBESol	PBE
ZnO	m_e	0.50082	0.47703	0.43436
	m_h	-2.83155	-2.95771	-2.53245
TiO_2	m_e	1.0911	0.83721	0.97667
	m_h	-3.77219	-2.53481	-2.20509

D. MOBILITY

In simulation, the mobility of electrons and holes is mainly calculated using the Boltzmann Transport theory [69]. Nevertheless, we calculated the mobility in this scientific work using the deformation potential theory [70]. In the Shockley-Barden theory, mobility is determined depending on the change in crystal size and band structure when mechanical force is applied to the crystal. According to the deformation potential theory, the mobility of electrons and holes is calculated using equation 10 [71].

$$\mu = \frac{(8\pi)^{\frac{1}{2}} h^4 e C_{ij}}{3 (m^*)^{\frac{5}{2}} (k_b T)^{\frac{3}{2}} E_{ij}^2} \tag{10}$$

where: e is the electron charge, T is the absolute temperature, k_b is the Boltzmann constant, C_{ij} is the elastic constant of the crystal, and E_{ij} is the energy change per unit volume.

TABLE 4. Important parameters calculated using PBE functional to determine the electron and hole mobilities.

	ZnO	TiO_2
V_0, A^3	50.230723	66.350264
E_{g0}, eV	0.518	1.728
V, A^3	47.594818	62.449209
E_g, eV	0.759	1.871
Bulk modulus, GPa	118.16481	208.26994

The energy change per unit volume was calculated using equation 11.

$$E_{ij} = \frac{dE}{\left(\frac{dV}{V_0}\right)} \tag{11}$$

where: dE is the energy difference before and after stress, V_0 is the initial volume of the crystal, and dV is the volume difference before and after stress.

Table 4 lists the parameters before and after applying the mechanical force calculated in PBE. ZnO and TiO_2 were applied mechanical force with the same 70 GPa in the (111) direction. After applying the mechanical force, the band gaps of ZnO and TiO_2 changed to 0.241 eV and 0.143 eV, respectively. Their crystal volume has changed to 2.64 A^3 and 3.9 A^3, respectively. The electron and hole mobilities of ZnO and TiO2 have been calculated using the theory of deformation potential and the parameters listed in Table 4. The calculated electron mobility for ZnO is 430.72 $cm^2V^{-1}s^{-1}$, and its calculated hole mobility is 5.25 $cm^2V^{-1}s^{-1}$. For TiO2, the calculated electron mobility is 355.27 $cm^2V^{-1}s^{-1}$, and its calculated hole mobility is 46.38 $cm^2V^{-1}s^{-1}$. In experiment, the electron and hole mobilities in ZnO are equal to 205 $cm^2V^{-1}s^{-1}$ [72] and 70 $cm^2V^{-1}s^{-1}$ [73]. The electronic mobility of ZnO calculated by PBE is almost 2 times larger than the experimental result, and the hole is 13 times smaller. In experiment, electron and hole mobilities in TiO_2 are 18.6 $cm^2V^{-1}s^{-1}$ [74] and 3.1 $cm^2V^{-1}s^{-1}$ [75], respectively. Therefore, the mobility of electrons and holes in TiO_2 calculated in PBE is 10 times larger than the experimental results. However, the fact that the electron mobility is significantly greater than the hole mobility for both materials, it satisfies the experimental results. Therefore, TiO_2 and ZnO tend to be n-type semiconductors [76].

E. OPTICAL PARAMETERS

Optical properties of materials are calculated in CASTEP mainly usingthe theory of Khon-Sham orbitals [77]. By the transmission of electrons in orbitals due to the photon electric field, it is possible to calculate the imaginary part of dielectric functions. The real and imaginary parts of dielectric function are related by the Kramers-Kronig transformation [78]. Therefore, the real part of the dielectric constant can be found through the imaginary part. The dielectric constant is determined from the real part of the dielectric function. When PW91, PBESol, PBE functionals were used, the dielectric constant was 11, 11.5, 8.5 for ZnO and 9.5, 10, 9 for TiO_2, respectively. In the experiment, depending on the synthesis method, the dielectric constants of ZnO and TiO_2 are equal to 8.17-9.34 [79] and 23-63.7 [80]. The dielectric constant of ZnO calculated in PBE satisfied the experimental result. If the synthesized TiO_2 is thermally treated, its dielectric constant would be 12.3 [81]. If we compare the dielectric constant of sufficiently thermally treated TiO2 with the simulation results, the simulation can satisfy the experimental results. When TiO_2 and ZnO are simulated as ETL layers in perovskite solar cells, their dielectric constant is mostly chosen 9 [82] or 10 [83]. This proves that our simulation results are partially correct.

One of the main optical properties of the material is the complex refractive index. Because it is possible to determine the absorption, reflection and transmission in the material [84] with the help of the complex refractive index. The complex refractive index is determined using equation 12.

$$\begin{cases} \varepsilon_1 = n^2 - k^2 \\ \varepsilon_2 = 2nk \end{cases} \tag{12}$$

where: ε_1 is the real part and ε_2 is the imaginary part of the complex permittivity.

Figure 4 shows the wavelength dependence of the complex refractive index of ZnO and TiO2 calculated using formula 7 and the dielectric function determined in PBE. The average refractive index of ZnO was equal to 2. In the experiment, the average refractive index of ZnO is also equal to 2 [85]. In addition, the complex refractive index of ZnO does not change dramatically depending on the wavelength of light [86] as our simulation results. As the wavelength increased from 100 nm to 450 nm, the refractive index of TiO_2 increased from 1 to 3.4. Then, when the wavelength increased to 900 nm, the refractive index decreased to 2.8. In the experiment, the refractive index of TiO2 is equal to 2.8 [87]. The imaginary part of the complex refractive index of ZnO was greater than 1 in the short wavelength, and less than 0.5 in the visible field. This proves that ZnO mainly absorbs light in the short ultraviolet range. In the wavelength range from 100 nm to 420 nm, the imaginary part of the complex refractive index of TiO_2 was found to be greater than 1.5, and it was found to be very small in the visible spectrum. Therefore, TiO2 absorbs light in UV spectrum more than ZnO.

F. HETEROJUNCTION SOLAR CELL

In experiment, the optic and emitter layers can be removed by chemically treating the surface of an industrially produced silicon-based solar cell to get p-type silicon. A ZnO/Si and TiO_2/Si heterojunction solar cell can be created by chemically preparing ZnO and TiO_2 and depositing them on p-type silicon using the Sol-Gel method [88]. In this paper, we used the TCAD simulation method to study

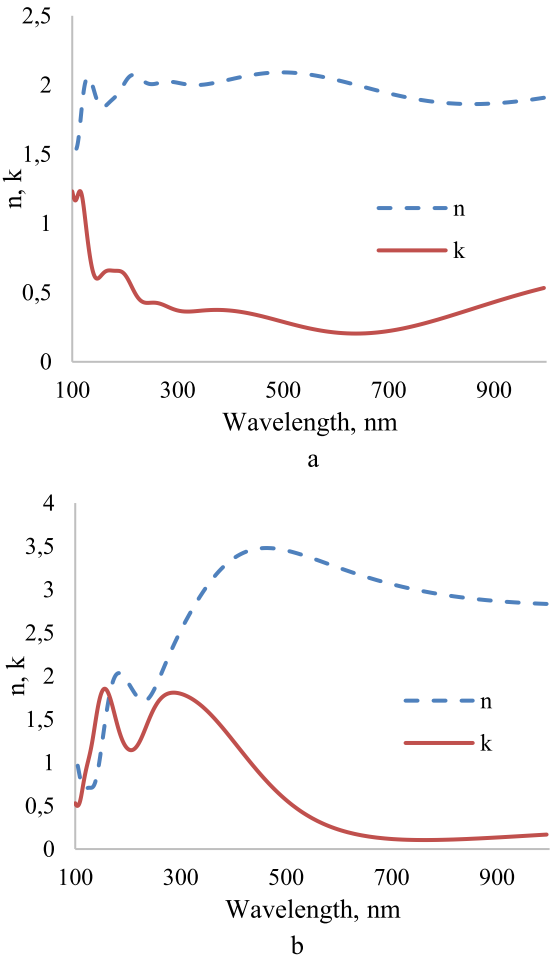

FIGURE 4. Dependence of the real and imaginary parts of the refractive indices of ZnO (a) and TiO_2 (b) calculated in the PBE functional on the light wavelength.

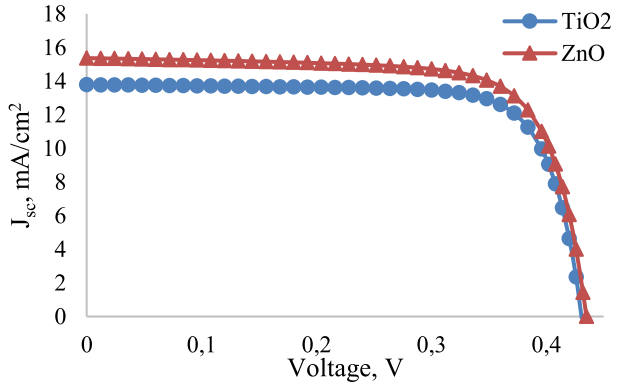

FIGURE 5. I-V characteristics of the ZnO/Si and TiO_2/Si heterojunction solar cell with an emitter layer thickness of 1 μm.

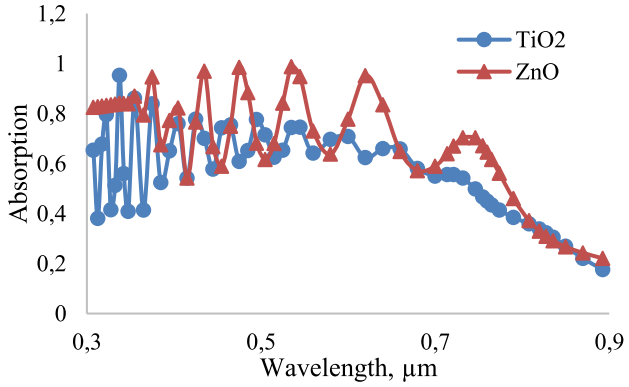

FIGURE 6. Spectral characteristics of a ZnO/Si and TiO_2/Si heterojunction solar cell with an emitter layer thickness of 1 μm.

heterojunction solar cells. The base of the solar cell is 10 μm and the emitter layer is 1 μm. Figure 5 shows the I-V characteristics of ZnO/Si and TiO_2/Si solar cells. The short circuit of ZnO/Si and TiO_2/Si are 15.37 mA/cm^2 and 13.78 mA/cm^2, respectively. The operating voltage is 0.435 V and 0.432 V respectively. The short circuit current is very low because the base thickness is 10 μm. The short circuit current of the solar cell is directly proportional to the thickness of the base.

When ZnO and TiO_2 are coated on the silicon surface, the n-MeO/p-Si heterojunction solar cell should absorb a wider spectrum of light than the n-Si/p-Si solar cell as the absorption spectra of MeO and Si are different. Figure 6 shows the dependence of the absorption coefficient of ZnO/Si and TiO_2/Si solar cells on the wavelength of light. Heterojunction solar cell absorb light well in the ultraviolet and visible fields. Because, according to Figure 4, ZnO and TiO_2 mainly absorb light in the ultraviolet range. Silicon mainly absorbs light in the visible range.

The fact that the absorption coefficient of ZnO/Si is greater than that of TiO_2/Si proves that its short-circuit current is greater. A wave appeared in the absorption spectrum of TiO_2 and ZnO. The reason for this is that internal interference [89] occurs in the emitter layer. If we choose the thickness of the emitter layer correctly, we can reduce the wave in the spectrum and increase the short circuit current. Figure 7 shows the dependence of the short-circuit current of heterojunction solar cells on the thickness of the emitter layer. The thickness of the emitter layer is 0.5-1.5 μm in industrial homojunction silicon-based solar cells [90]. Since metal oxides simultaneously functioned as an emitter layer and an anti-reflection layer, their optimal thickness was 80 nm for ZnO/Si and 40 nm for TiO2/Si. Therefore, the maximum short-circuit current of ZnO/Si and TiO_2/Si heterojunction solar cells is 18 mA/cm^2 and 15.3 mA/cm^2. Between 40 nm and 1200 nm of the emitter layer, the short-circuit current of ZnO/Si is larger than that of TiO_2/Si solar cell. In this size, the short-circuit current of a silicon-based homojunction solar cell is 13.5 mA/cm^2. Therefore, if we cover the silicon surface with 80 nm thick ZnO or 40 nm thick TiO_2 as an emitter layer, its short circuit current increases to 4.5 mA/cm^2 and 1.8 mA/cm^2, respectively.

Metal oxides can also act as transparent contacts for silicon-based solar cells. It is possible to analyze the resistive parameters of the solar cell by the value of the fill factor of the solar cell. Figure 8 shows the dependence of the fill factor of heterojunction solar cells on the thickness of the emitter layer.

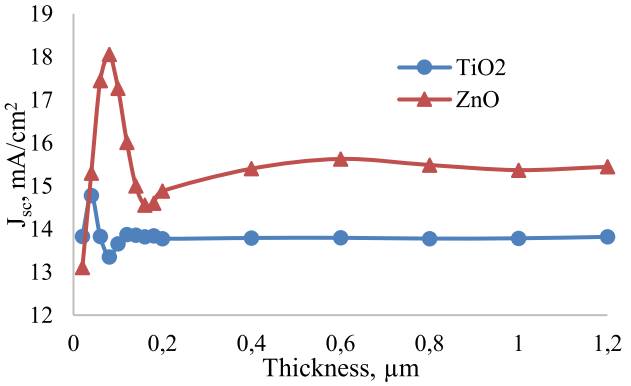

FIGURE 7. Dependence of the short-circuit current of ZnO/Si and TiO_2/Si solar cells on the thickness of the emitter layer.

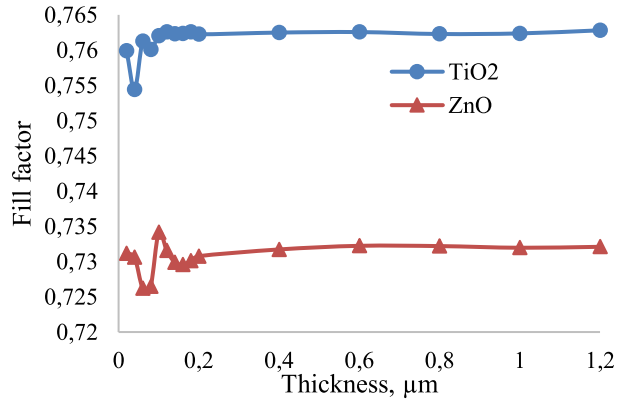

FIGURE 8. The dependence of the fill factor of ZnO/Si and TiO_2/Si solar cells on the thickness of the emitter layer.

The average fill factor of ZnO/Si and TiO_2/Si solar cells was 0.73 and 0.76. At small thicknesses, the fill factor changed dramatically, but remained almost unchanged in the range from 0.2 μm to 1.2 μm. Therefore, according to the obtained results, TiO_2 has a good effect on the resistive properties of the solar cell since it has higher fill factor. Hence, TiO_2 can be used as a transparent contact.

IV. CONCLUSION

In this research study, the physical properties of TiO_2 and ZnO, two widely used metal oxides were calculated using the CASTEP code. The main results obtained, from PBE, PBESol and PW91 functionals of GGA were compared and the optimal functional for metal oxides was identified. The best functionals for determining crystal lattice constants were found to be PBE for ZnO and PBESol for TiO_2. The band structure calculation showed that both ZnO and TiO2 are direct semiconductors. According to optical properties, it was revealed that ZnO and TiO_2 mainly absorb ultraviolet light. That's why, they are transparent and therefore for use in ultraviolet light diode. The effective mass of electrons in ZnO and TiO_2 is smaller than that of holes. Electron mobility is greater than that of the hole for both of metal oxides. Which making both materials primarily n-type semiconductor. This makes them ideal for use as an ETL layer in perovskite and organic solar cells, as well as an emitter layer in silicon-based solar cells. The DFT results of ZnO and TiO_2 led to the conclusion that n-ZnO/p-Si and n-TiO_2/p-Si heterojunction solar cells can be formed and were modeled using TCAD software. The optimal thicknesses of ZnO and TiO_2 were found to be 80 nm and 40 nm, respectively. The average fill factors of TiO_2/Si and ZnO/Si solar cells were 0.76 and 0.73, respectively. Therefore, if we consider that fill factor of TiO_2/Si is higher than that of ZnO/Si and short circuit current of ZnO/Si is greater than that of TiO_2/Si. This suggests that TiO_2 may be used as a transparent contact and ZnO as an emitter layer in a silicon-based solar cell.

In the future, we plan to conduct research on other metal oxides to identify the most suitable candidate for the emitter layer in silicon heterojunction solar cells, using an atom-to-device simulation chain. Besides, we will investigate the impact of different metal nanoparticles on the photoelectric properties of these metal oxides.

REFERENCES

[1] R. M. Swanson, "Approaching the 29% limit efficiency of silicon solar cells," in *Proc. 31st IEEE Photovoltaic Spec. Conf.*, 2005, pp. 889–894, doi: 10.1109/PVSC.2005.1488274.

[2] F. Fertig, B. Kloter, I. Hoger, K. Petter, E. Jarzembowski, M. Junghanel, C. Klenke, A. Weihrauch, M. Schley, K. Kim, and A. Schwabedissen, "Q CELLS >24% silicon solar cells with mass-production processes," *IEEE J. Photovolt.*, vol. 12, no. 1, pp. 22–25, Jan. 2022, doi: 10.1109/JPHOTOV.2021.3112122.

[3] B. H. Hamadani, "Understanding photovoltaic energy losses under indoor lighting conditions," *Appl. Phys. Lett.*, vol. 117, no. 4, Jul. 2020, Art. no. 043904, doi: 10.1063/5.0017890.

[4] C. Ji, W. Liu, Y. Bao, X. Chen, G. Yang, B. Wei, F. Yang, and X. Wang, "Recent applications of antireflection coatings in solar cells," *Photonics*, vol. 9, no. 12, p. 906, Nov. 2022, doi: 10.3390/PHOTONICS9120906.

[5] J. Gulomov and R. Aliev, "Influence of the angle of incident light on the performance of textured silicon solar cells," *J. Nano- Electron. Phys.*, vol. 13, no. 6, pp. 1–5, 2021, doi: 10.21272/JNEP.13(6).06036.

[6] J. Day, S. Senthilarasu, and T. K. Mallick, "Improving spectral modification for applications in solar cells: A review," *Renew Energy*, vol. 132, pp. 186–205, Mar. 2019, doi: 10.1016/J.RENENE.2018.07.101.

[7] W. Wang, S. Wu, K. Reinhardt, Y. Lu, and S. Chen, "Broadband light absorption enhancement in thin-film silicon solar cells," *Nano Lett.*, vol. 10, no. 6, pp. 2012–2018, Jun. 2010, doi: 10.1021/nl904057p.

[8] X. Huang, S. Han, W. Huang, and X. Liu, "Enhancing solar cell efficiency: The search for luminescent materials as spectral converters," *Chem. Soc. Rev.*, vol. 42, no. 1, pp. 173–201, Dec. 2012, doi: 10.1039/C2CS35288E.

[9] B. Ai, Z. Fan, and Z. J. Wong, "Plasmonic-perovskite solar cells, light emitters, and sensors," *Microsystems. Nanoeng.*, vol. 1, vol. 8, no. 1, pp. 1–28, Jan. 2022, doi: 10.1038/s41378-021-00334-2.

[10] U. Sikder and A. Haque, "Optimization of idealized quantum dot intermediate band solar cells considering spatial variation of generation rates," *IEEE Access*, vol. 1, pp. 363–370, 2013, doi: 10.1109/ACCESS.2013.2265094.

[11] J. Gulomov and R. Aliev, "Numerical analysis of the effect of illumination intensity on photoelectric parameters of the silicon solar cell with various metal nanoparticles," *Nanosyst. Phys. Chem. Math.*, vol. 12, no. 5, pp. 569–574, Oct. 2021, doi: 10.17586/2220-8054-2021-12-5-569-574.

[12] J. Gulomov and O. Accouche, "Gold nanoparticles introduced ZnO/perovskite/silicon heterojunction solar cell," *IEEE Access*, vol. 10, pp. 119558–119565, 2022, doi: 10.1109/ACCESS.2022.3221875.

[13] C. Liu, Y. Lu, R. Shen, Y. Dai, X. Yu, K. Liu, and S. Lin, "Dynamics and physical process of hot carriers in optoelectronic devices," *Nano Energy*, vol. 95, May 2022, Art. no. 106977, doi: 10.1016/J.NANOEN.2022.106977.

[14] I. H. Choi, M. S. Kim, C. Kang, and J. S. Lee, "Ultrafast real-time tracing of surface electric field generated via hot electron transport in polar semiconductors," *Appl. Surf. Sci.*, vol. 571, Jan. 2022, Art. no. 151279, doi: 10.1016/J.APSUSC.2021.151279.

[15] J. Y. Huang, Y. Wang, G. T. Fei, S. H. Xu, B. Wang, and Z. Zeng, "Dual-functional antireflection and down-shifting coating for Si solar cells," *Colloids Surf. A, Physicochem. Eng. Aspects*, vol. 652, Nov. 2022, Art. no. 129907, doi: 10.1016/J.COLSURFA.2022.129907.

[16] N. Chander, S. K. Sardana, P. K. Parashar, A. F. Khan, S. Chawla, and V. K. Komarala, "Improving the short-wavelength spectral response of silicon solar cells by spray deposition of YVO_4:Eu^{3+} downshifting phosphor nanoparticles," *IEEE J. Photovolt.*, vol. 5, no. 5, pp. 1373–1379, Sep. 2015, doi: 10.1109/JPHOTOV.2015.2438633.

[17] M. Hu, J. Chen, Z. Y. Li, L. Au, G. V. Hartland, X. Li, M. Marquez, and Y. Xia, "Gold nanostructures: Engineering their plasmonic properties for biomedical applications," *Chem. Soc. Rev.*, vol. 35, no. 11, pp. 1084–1094, Oct. 2006, doi: 10.1039/B517615H.

[18] E. Van Kerschaver and G. Beaucarne, "Back-contact solar cells: A review," *Prog. Photovolt., Res. Appl.*, vol. 14, no. 2, pp. 107–123, Dec. 2006, doi: 10.1002/PIP.657.

[19] S. W. Glunz and F. Feldmann, "SiO_2 surface passivation layers—A key technology for silicon solar cells," *Sol. Energy Mater. Sol. Cells*, vol. 185, pp. 260–269, Oct. 2018, doi: 10.1016/J.SOLMAT.2018.04.029.

[20] M. Cui, J. Ma, and X. Wu, "Multilayer SiN_x: H films as passivation and anti-reflection coating for industrial PERC solar cells," *Optik*, vol. 268, Oct. 2022, Art. no. 169841, doi: 10.1016/J.IJLEO.2022.169841.

[21] J. Gulomov, O. Accouche, R. Aliev, B. Neji, R. Ghandour, I. Gulomova, and M. Azab, "Geometric optimization of perovskite solar cells with metal oxide charge transport layers," *Nanomaterials*, vol. 12, no. 15, p. 2692, Aug. 2022, doi: 10.3390/NANO12152692.

[22] H. Yao and J. Hou, "Recent advances in single-junction organic solar cells," *Angew. Chem.*, vol. 134, no. 37, Sep. 2022, Art. no. e202209021, doi: 10.1002/ANGE.202209021.

[23] D. Lee, A. Lee, and H. D. Kim, "IZO/ITO double-layered transparent conductive oxide for silicon heterojunction solar cells," *IEEE Access*, vol. 10, pp. 77170–77175, 2022, doi: 10.1109/ACCESS.2022.3192646.

[24] T. Dai, Q. Cao, L. Yang, M. H. Aldamasy, M. Li, Q. Liang, H. Lu, Y. Dong, and Y. Yang, "Strategies for high-performance large-area perovskite solar cells toward commercialization," *Crystals*, vol. 11, no. 3, p. 295, Mar. 2021, doi: 10.3390/CRYST11030295.

[25] X. Gu, X. Lai, Y. Zhang, T. Wang, W. L. Tan, C. R. McNeill, Q. Liu, P. Sonar, F. He, W. Li, and C. Shan, "Organic solar cell with efficiency over 20% and VOC exceeding 2.1 V enabled by tandem with all-inorganic perovskite and thermal annealing-free process," *Adv. Sci.*, vol. 9, no. 28, Oct. 2022, Art. no. 2200445, doi: 10.1002/ADVS.202200445.

[26] N. Kant and P. Singh, "Review of next generation photovoltaic solar cell technology and comparative materialistic development," *Mater. Today Proc.*, vol. 56, pp. 3460–3470, Jan. 2022, doi: 10.1016/J.MATPR.2021.11.116.

[27] Y. Lee, H. M. Kim, J. Kim, and J. Jang, "Remarkable lifetime improvement of quantum-dot light emitting diodes by incorporating Rubidium carbonate in metal-oxide electron transport layers," *J. Mater. Chem. C*, vol. 7, no. 32, pp. 10082–10091, Aug. 2019, doi: 10.1039/C9TC02683E.

[28] V. D. Patel and D. Gupta, "Solution-processed metal-oxide based hole transport layers for organic and perovskite solar cell: A review," *Mater. Today Commun.*, vol. 31, Jun. 2022, Art. no. 103664, doi: 10.1016/J.MTCOMM.2022.103664.

[29] J. Kaupuzs, A. Medvids, P. Onufrijevs, and H. Mimura, "Origin of *n*-type conductivity in ZnO crystal and formation of Zn and ZnO nanoparticles by laser radiation," *Opt. Laser Technol.*, vol. 111, pp. 121–128, Apr. 2019, doi: 10.1016/J.OPTLASTEC.2018.09.037.

[30] F. Menchini, M. L. Grilli, T. Dikonimos, A. Mittiga, L. Serenelli, E. Salza, R. Chierchia, and M. Tucci, "Application of NiO_x thin films as *p*-type emitter layer in heterojunction solar cells," *Phys. Status Solidi (C)*, vol. 13, nos. 10–12, pp. 1006–1010, Dec. 2016, doi: 10.1002/PSSC.201600121.

[31] T. T. Nguyen, M. Patel, and J. Kim, "All-inorganic metal oxide transparent solar cells," *Sol. Energy Mater. Sol. Cells*, vol. 217, Nov. 2020, Art. no. 110708, doi: 10.1016/J.SOLMAT.2020.110708.

[32] M. Patel, H.-S. Kim, J. Kim, J.-H. Yun, S. J. Kim, E. H. Choi, and H.-H. Park, "Excitonic metal oxide heterojunction (NiO/ZnO) solar cells for all-transparent module integration," *Sol. Energy Mater. Sol. Cells*, vol. 170, pp. 246–253, Oct. 2017, doi: 10.1016/J.SOLMAT.2017.06.006.

[33] M. Mousa, F. Z. Amer, R. I. Mubarak, and A. Saeed, "Simulation of optimized high-current tandem solar-cells with efficiency beyond 41%," *IEEE Access*, vol. 9, pp. 49724–49737, 2021, doi: 10.1109/ACCESS.2021.3069281.

[34] Y. Jestin, S. Chandra, B. Cass, H. Ahmed, and S. J. McCormack, "Down-shifting of the incident light for photovoltaic applications," in *Comprehensive Renewable Energy*. 2022, pp. 534–560, doi: 10.1016/B978-0-12-819727-1.00126-6.

[35] F. Dimroth and S. Kurtz, "High-efficiency multijunction solar cells," *MRS Bull.*, vol. 32, no. 3, pp. 230–235, Jan. 2007, doi: 10.1557/mrs2007.27.

[36] K. Sveinbjornsson, B. Li, S. Mariotti, E. Jarzembowski, L. Kegelmann, A. Wirtz, F. Fruhauf, A. Weihrauch, R. Niemann, L. Korte, and F. Fertig, "Monolithic perovskite/silicon tandem solar cell with 28.7% efficiency using industrial silicon bottom cells," *ACS Energy Lett.*, vol. 7, no. 8, pp. 2654–2656, Aug. 2022, doi: 10.1021/acsenergylett.2c01358.

[37] T. Shawky, M. H. Aly, and M. Fedawy, "Performance analysis and simulation of c-Si/SiGe based solar cell," *IEEE Access*, vol. 9, pp. 75283–75292, 2021, doi: 10.1109/ACCESS.2021.3080391.

[38] M. Kohler, M. Pomaska, A. Zamchiy, A. Lambertz, W. Duan, F. Lentz, S. Li, V. Smirnov, T. Kirchartz, F. Finger, and U. Rau, "Optimization of transparent passivating contact for crystalline silicon solar cells," *IEEE J. Photovolt.*, vol. 10, no. 1, pp. 46–53, Jan. 2020, doi: 10.1109/JPHOTOV.2019.2947131.

[39] A. C. R. Fernendez, A. B. Schvval, M. J. Jimenez, G. F. Cabeza, and C. I. N. Morgade, "Comparative study of the effect of the Hubbard coefficient U on the properties of TiO_2 and ZnO," *Mater. Today Commun.*, vol. 27, Jun. 2021, Art. no. 102368, doi: 10.1016/J.MTCOMM.2021.102368.

[40] S. Sakthivel, B. Neppolian, M. V. Shankar, B. Arabindoo, M. Palanichamy, and V. Murugesan, "Solar photocatalytic degradation of azo dye: Comparison of photocatalytic efficiency of ZnO and TiO_2," *Sol. Energy Mater. Sol. Cells*, vol. 77, no. 1, pp. 65–82, Apr. 2003, doi: 10.1016/S0927-0248(02)00255-6.

[41] A. Pervez, K. Javed, Z. Iqbal, M. Shahzad, U. Khan, H. Latif, S. A. Shah, and N. Ahmad, "Fabrication and comparison of dye-sensitized solar cells by using TiO_2 and ZnO as photo electrode," *Optik*, vol. 182, pp. 175–180, Apr. 2019, doi: 10.1016/J.IJLEO.2018.12.044.

[42] J. Y. Huang, Y. Wang, G. T. Fei, S. H. Xu, Z. Zeng, and B. Wang, "TiO_2/ZnO double-layer broadband antireflective and down-shifting coatings for solar applications," *Ceram. Int.*, vol. 49, no. 7, pp. 11091–11100, Apr. 2023, doi: 10.1016/J.CERAMINT.2022.11.305.

[43] V. Milman, K. Refson, S. J. Clark, C. J. Pickard, J. R. Yates, S. P. Gao, P. J. Hasnip, M. I. J. Probert, A. Perlov, and M. D. Segall, "Electron and vibrational spectroscopies using DFT, plane waves and pseudopotentials: CASTEP implementation," *J. Mol. Struct., THEOCHEM*, vol. 954, pp. 22–35, Aug. 2010, doi: 10.1016/J.THEOCHEM.2009.12.040.

[44] J. Paier, R. Hirschl, M. Marsman, and G. Kresse, "The Perdew–Burke–Ernzerhof exchange-correlation functional applied to the G2–1 test set using a plane-wave basis set," *J. Chem. Phys.*, vol. 122, no. 23, Jun. 2005, Art. no. 234102, doi: 10.1063/1.1926272.

[45] J. P. Perdew, A. Ruzsinszky, G. I. Csonka, O. A. Vydrov, G. E. Scuseria, L. A. Constantin, X. Zhou, and K. Burke, "Restoring the density-gradient expansion for exchange in solids and surfaces," *Phys. Rev. Lett.*, vol. 100, no. 13, Apr. 2008, Art. no. 136406, doi: 0.1103/PhysRevLett.100.136406.

[46] Y. Wang and J. P. Perdew, "Correlation hole of the spin-polarized electron gas, with exact small-wave-vector and high-density scaling," *Phys. Rev. B, Condens. Matter*, vol. 44, p. 13298, Dec. 1991, doi: 10.1103/PhysRevB.44.13298.

[47] C. G. Broyden, "The convergence of a class of double-rank minimization algorithms 1. General considerations," *J. Math. Appl.*, vol. 6, no. 1, pp. 76–90, 1970, doi: 10.1093/IMAMAT/6.1.76.

[48] W. S. Morgan, J. J. Jorgensen, B. C. Hess, and G. L. W. Hart, "Efficiency of generalized regular K-point grids," *Comput. Mater. Sci.*, vol. 153, pp. 424–430, Oct. 2018, doi: 10.1016/J.COMMATSCI.2018.06.031.

[49] M. K. Abduvohidov, R. Aliev, and J. Gulomov, "A study of the influence of the base thickness on photoelectric parameterof silicon solar cells with the new TCAD algorithms," *Sci. Tech. J. Inf. Technol., Mech. Opt.*, vol. 21, no. 5, pp. 774–784, 2021, doi: 10.17586/2226-1494-2021-21-5-774-784.

[50] K. H. Lee, K. Araki, and M. Yamaguchi, "A mesh downsampling algorithm for equivalent circuit network simulation of multi-junction solar cells," *IEEE Access*, vol. 7, pp. 97208–97215, 2019, doi: 10.1109/ACCESS.2019.2930002.

[51] L. Chen and H. Bagci, "Steady-state simulation of semiconductor devices using discontinuous Galerkin methods," *IEEE Access*, vol. 8, pp. 16203–16215, 2020, doi: 10.1109/ACCESS.2020.2967125.

[52] S. N. Mohammad and A. V. Bemis, "The Einstein relation for degenerate semiconductors with nonuniform band structures," *IEEE Trans. Electron Devices*, vol. 39, no. 12, pp. 2826–2828, Dec. 1992, doi: 10.1109/16.168739.

[53] D. Nagy, G. Indalecio, A. J. Garcia-Loureiro, G. Espineira, M. A. Elmessary, K. Kalna, and N. Seoane, "Drift-diffusion versus Monte Carlo simulated ON-current variability in nanowire FETs," *IEEE Access*, vol. 7, pp. 12790–12797, 2019, doi: 10.1109/ACCESS.2019.2892592.

[54] K. R. McIntosh, M. D. Abbott, and B. A. Sudbury, "Ray tracing isotextured solar cells," *Energy Proc.*, vol. 92, pp. 122–129, Aug. 2016, doi: 10.1016/J.EGYPRO.2016.07.041.

[55] J. A. B. Faria, "The transfer matrix method: Analysis of nonuniform multiport systems," *IEEE Access*, vol. 8, pp. 23650–23662, 2020, doi: 10.1109/ACCESS.2020.2968575.

[56] T. Dennis, J. B. Schlager, and K. A. Bertness, "A novel solar simulator based on a supercontinuum laser for solar cell device and materials characterization," *IEEE J. Photovolt.*, vol. 4, no. 4, pp. 1119–1127, Jul. 2014, doi: 10.1109/JPHOTOV.2014.2321659.

[57] J. Gulomov, R. Aliev, and B. Urmanov, "Effect of the thickness on photoelectric parameters of a textured silicon solar cell," *J. Surf. Invest.*, vol. 16, no. 3, pp. 416–420, Jun. 2022, doi: 10.1134/S1027451022030375.

[58] U. Ozgur, "A comprehensive review of ZnO materials and devices," *J. Appl. Phys.*, vol. 98, no. 4, Aug. 2005, Art. no. 041301, doi: 10.1063/1.1992666.

[59] K. Sugiyama and Y. Takeuchi, "The crystal structure of rutile as a function of temperature up to 1600 °C," *Zeitschrift für Kristallographie-Crystalline Mater.*, vol. 194, nos. 1–4, pp. 305–314, Aug. 1991, doi: 10.1524/ZKRI.1991.194.14.305.

[60] R. R. Reeber, "Lattice parameters of ZnO from 4.2° to 296 °K," *J. Appl. Phys.*, vol. 41, no. 13, p. 5063, Dec. 2003, doi: 10.1063/1.1658600.

[61] F. Mouhat and F. X. Coudert, "Necessary and sufficient elastic stability conditions in various crystal systems," *Phys. Rev. B, Condens. Matter*, vol. 90, no. 22, Dec. 2014, Art. no. 224104, doi: 10.1103/PhysRevB.90.224104.

[62] K. Davis, R. Yarbrough, M. Froeschle, J. White, and H. Rathnayake, "Band gap engineered zinc oxide nanostructures via a sol-gel synthesis of solvent driven shape-controlled crystal growth," *RSC Adv.*, vol. 9, no. 26, pp. 14638–14648, May 2019, doi: 10.1039/C9RA02091H.

[63] C. Dette, M. A. Pérez-Osorio, C. S. Kley, P. Punke, C. E. Patrick, P. Jacobson, F. Giustino, S. J. Jung, and K. Kern, "TiO_2 anatase with a bandgap in the visible region," *Nano Lett.*, vol. 14, no. 11, pp. 6533–6538, Nov. 2014, doi: 10.1021/nl503131s.

[64] J. H. Yuan, Q. Chen, L. R. C. Fonseca, M. Xu, K. H. Xue, and X. S. Miao, "GGA-1/2 self-energy correction for accurate band structure calculations: The case of resistive switching oxides," *J. Phys. Commun.*, vol. 2, no. 10, Oct. 2018, Art. no. 105005, doi: 10.1088/2399-6528/AADE7E.

[65] J. Gulomov, O. Accouche, Z. Al Barakeh, R. Aliev, I. Gulomova, and B. Neji, "Atom-to-device simulation of MoO_3/Si heterojunction solar cell," *Nanomaterials*, vol. 12, no. 23, p. 4240, Nov. 2022, doi: 10.3390/NANO12234240.

[66] D. P. Norton, Y. W. Heo, M. P. Ivill, K. Ip, S. J. Pearton, M. F. Chisholm, and T. Steiner, "ZnO: Growth, doping & processing," *Mater. Today*, vol. 7, no. 6, pp. 34–40, Jun. 2004, doi: 10.1016/S1369-7021(04)00287-1.

[67] V. Mikhelashvili and G. Eisenstein, "Effects of annealing conditions on optical and electrical characteristics of titanium dioxide films deposited by electron beam evaporation," *J. Appl. Phys.*, vol. 89, no. 6, p. 3256, Mar. 2001, doi: 10.1063/1.1349860.

[68] S. Dong, S. Xia, C. Wang, J. Dong, T. Wang, R. Li, Z. Ren, D. Dai, X. Yang, and C. Zhou, "Valence band of rutile TiO_2(110) investigated by polarized-light-based angle-resolved photoelectron spectroscopy," *J. Phys. Chem. Lett.*, vol. 13, no. 10, pp. 2299–2305, Mar. 2022, doi: 10.1021/acs.jpclett.2c00142.

[69] A. Paussa and D. Esseni, "An exact solution of the linearized Boltzmann transport equation and its application to mobility calculations in graphene bilayers," *J. Appl. Phys.*, vol. 113, no. 9, Mar. 2013, Art. no. 093702, doi: 10.1063/1.4793634.

[70] J. Bardeen and W. Shockley, "Deformation potentials and mobilities in non-polar crystals," *Phys. Rev.*, vol. 80, no. 1, p. 72, Oct. 1950, doi: 10.1103/PhysRev.80.72.

[71] J. Xi, M. Long, L. Tang, D. Wang, and Z. Shuai, "First-principles prediction of charge mobility in carbon and organic nanomaterials," *Nanoscale*, vol. 4, no. 15, pp. 4348–4369, Jul. 2012, doi: 10.1039/C2NR30585B.

[72] D. C. Look, D. C. Reynolds, J. R. Sizelove, R. L. Jones, C. W. Litton, G. Cantwell, and W. C. Harsch, "Electrical properties of bulk ZnO," *Solid State Commun.*, vol. 105, no. 6, pp. 399–401, Feb. 1998, doi: 10.1016/S0038-1098(97)10145-4.

[73] A. Tsukazaki, A. Ohtomo, T. Onuma, M. Ohtani, T. Makino, M. Sumiya, K. Ohtani, S. F. Chichibu, S. Fuke, Y. Segawa, and H. Ohno, "Repeated temperature modulation epitaxy for *p*-type doping and light-emitting diode based on ZnO," *Nature Mater.*, vol. 1, vol. 4, no. 1, pp. 42–46, Dec. 2004, doi: 10.1038/nmat1284.

[74] T. S. Krasienapibal, T. Fukumura, Y. Hirose, and T. Hasegawa, "Improved room temperature electron mobility in self-buffered anatase TiO_2 epitaxial thin film grown at low temperature," *Jpn. J. Appl. Phys.*, vol. 53, no. 9, Aug. 2014, Art. no. 090305, doi: 10.7567/JJAP.53.090305.

[75] A. Panepinto, J. Dervaux, P. A. Cormier, M. Boujtita, F. Odobel, and R. Snyders, "Synthesis of *p*-type N-doped TiO_2 thin films by co-reactive magnetron sputtering," *Plasma Processes Polym.*, vol. 17, no. 3, Mar. 2020, Art. no. 1900203, doi: 10.1002/PPAP.201900203.

[76] H. Yanagida and M. Miyayama, "Oxides," in *Concise Encyclopedia of Advanced Ceramic Materials*. 1991, pp. 340–346, doi: 10.1016/B978-0-08-034720-2.50094-0.

[77] S. Hamel, P. Duffy, M. E. Casida, and D. R. Salahub, "Kohn–Sham orbitals and orbital energies: Fictitious constructs but good approximations all the same," *J. Electron Spectrosc. Rel. Phenomena*, vol. 123, nos. 2–3, pp. 345–363, May 2002, doi: 10.1016/S0368-2048(02)00032-4.

[78] B. Johs and J. S. Hale, "Dielectric function representation by B-splines," *Phys. Status Solidi (A)*, vol. 205, no. 4, pp. 715–719, Apr. 2008, doi: 10.1002/PSSA.200777754.

[79] S. V. Vegesna, V. J. Bhat, D. Burger, J. Dellith, I. Skorupa, O. G. Schmidt, and H. Schmidt, "Increased static dielectric constant in ZnMnO and ZnCoO thin films with bound magnetic polarons," *Sci. Rep.*, vol. 10, p. 6698, Apr. 2020, doi: 10.1038/s41598-020-63195-1.

[80] A. Wypych, I. Bobowska, M. Tracz, A. Opasinska, S. Kadlubowski, A. Krzywania-Kaliszewska, J. Grobelny, and P. Wojciechowski, "Dielectric properties and characterisation of titanium dioxide obtained by different chemistry methods," *J. Nanomater.*, vol. 2014, pp. 1–9, Jan. 2014, doi: 10.1155/2014/124814.

[81] C. T. Dervos, E. Thirios, J. Novacovich, P. Vassiliou, and P. Skafidas, "Permittivity properties of thermally treated TiO_2," *Mater. Lett.*, vol. 58, no. 9, pp. 1502–1507, Mar. 2004, doi: 10.1016/J.MATLET.2003.10.012.

[82] F. Azri, A. Meftah, N. Sengouga, and A. Meftah, "Electron and hole transport layers optimization by numerical simulation of a perovskite solar cell," *Sol. Energy*, vol. 181, no. 18, pp. 372–378, Mar. 2019, doi: 10.1016/J.SOLENER.2019.02.017.

[83] M. A. Rahman, "Enhancing the photovoltaic performance of Cd-free Cu_2ZnSnS_4 heterojunction solar cells using SnS HTL and TiO_2 ETL," *Sol. Energy*, vol. 215, pp. 64–76, Feb. 2021, doi: 10.1016/J.SOLENER.2020.12.020.

[84] S. Y. El-Zaiat, "Determination of the complex refractive index of a thick slab material from its spectral reflectance and transmittance at normal incidence," *Optik*, vol. 124, no. 2, pp. 157–161, Jan. 2013, doi: 10.1016/J.IJLEO.2011.11.039.

[85] A. M. Alsaad, Q. M. Al-Bataineh, A. A. Ahmad, Z. Albataineh, and A. Telfah, "Optical band gap and refractive index dispersion parameters of boron-doped ZnO thin films: A novel derived mathematical model from the experimental transmission spectra," *Optik*, vol. 211, Jun. 2020, Art. no. 164641, doi: 10.1016/J.IJLEO.2020.164641.

[86] O. Aguilar, S. de Castro, M. P. F. Godoy, M. Rebello, and S. Dias, "Optoelectronic characterization of $Zn_{1-x}Cd_xO$ thin films as an alternative to photonic crystals in organic solar cells," *Opt. Mater. Exp.*, vol. 9, no. 9, pp. 3638–3648, Sep. 2019, doi: 10.1364/OME.9.003638.

[87] W. Wang and L. Cui, "Optical properties of anatase and rutile TiO_2 films deposited by using a pulsed laser," *Appl. Opt.*, vol. 60, no. 27, pp. 8453–8457, Sep. 2021, doi: 10.1364/AO.437646.

[88] B. Jang, H. Kang, W. Y. Lee, J. H. Bae, I. M. Kang, K. Kim, H. J. Kwon, and J. Jang, "Enhancement mode flexible SnO_2 thin film transistors via a UV/Ozone-assisted sol-gel approach," *IEEE Access*, vol. 8, pp. 123013–123018, 2020, doi: 10.1109/ACCESS.2020.3007372.

[89] D. Poitras and J. A. Dobrowolski, "Toward perfect antireflection coatings. 2. Theory," *Appl. Opt.*, vol. 43, no. 6, pp. 1286–1295, Feb. 2004, doi: 10.1364/AO.43.001286.
[90] T. Dullweber and J. Schmidt, "Industrial silicon solar cells applying the passivated emitter and rear cell (PERC) concept—A review," *IEEE J. Photovolt.*, vol. 6, no. 5, pp. 1366–1381, Sep. 2016, doi: 10.1109/JPHOTOV.2016.2571627.

JASURBEK GULOMOV was born in Andijan, Uzbekistan, in 1999. He received the B.S. degree in physics from Andijan State University, Uzbekistan, in 2021, where he is currently pursuing the master's degree in physics, with a focus on renewable energy sources and environmental sustainability. He is currently a Researcher with the Renewable Energy Sources Laboratory, Andijan State University. He is the author of 16 articles and seven inventions. His research interests include numerical simulation, nanoplasmonic solar cells, metal nanoparticles, metal oxides, heterojunction solar cells, computational material science, and programming. He is the Holder of a National Scholarship after being named Mirzo Ulugbek and was a Winner of Student of the Year, in 2021. Besides, he was a Winner of President Scholarship, in 2022.

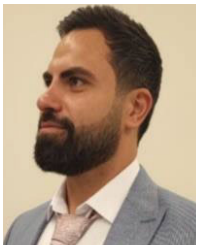

OUSSAMA ACCOUCHE (Associate Member, IEEE) received the degree in electrical engineering from Lebanese University, Beirut, Lebanon, in 2011, and the master's and Ph.D. degrees in smart grids from Grenoble-Alpes University, Grenoble, France, in 2016. He has several years of industrial and international experience, including France, Italy, and Japan, as a supervisor engineer. Since September 2018, he has been an Assistant Professor with the Electrical Engineering Department, American University of the Middle East, Egaila, Kuwait. His research interests include smart grids, renewable energies, solar cells, artificial intelligence, and smart cities.

RAYIMJON ALIEV was born in 1958. He received the Graduate degree in physics from Andijan State University named after Z. M. Bobur, in 1979, the Ph.D. degree in physics and mathematics from the National University of Science and Technology (MISiS), Russia, in 1988, and the D.Sc. degree in technics from the Physical and Technical Institute, Academy of Science of Uzbekistan, in 2002. Currently, he is a Professor with the Physics Department, Andijan State University, and the Head of the Renewable Energy Sources Laboratory. He is the author of 45 articles and 15 inventions. His research interests include solar cells, nanoplasmonics, simulation, nanostructured solar cells, silicon, textures, antireflection coatings, hybrid solar-wind, and solar-hydro energy sources.

RAYMOND GHANDOUR (Senior Member, IEEE) received the B.Eng. degree in computer and communication engineering (industrial computing and robotics field) from Holy Spirit University, Kaslik, Lebanon, in 2007, the M.S. degree in industrial control from Lebanese University, Beirut, Lebanon, in 2008, the M.S. degree in information technology and systems from the University of Technology of Compiegne, France, in 2008, the Ph.D. degree in automatic control from the University of Technology of Compiegne, France, in 2011, and the master's degree from the IAE Business School, Lille, in 2015, through the Development of Innovative Projects and Startups. In December 2011, he was a Postdoctoral Researcher with Polytechnic University—Hauts de France, Valenciennes, France. In December 2012, he was a Postdoctoral Researcher with CETIM and the University of Technology of Compiegne. He joined the ALTRAN Group—ALTRAN Technologies—North Division, Lille, France, as the Director of Research and Development, in April 2013. In 2016, he founded Innovation Universe Consulting Company to support innovative ideas and transform them into companies. He is currently an Associate Professor with the American University of the Middle East, Kuwait. He has been conducting and managing research in different areas, including control of hybrid vehicles, vehicle dynamics, signal processing, driving assistance systems, modeling and control of nonlinear systems, and green energy.

IRODAKHON GULOMOVA was born in Andijan, Uzbekistan, in 1999. She received the B.S. degree in physics from Andijan State University, Uzbekistan, in 2022, where she is currently pursuing the master's degree in physics of renewable energy sources and sustainable environment. Besides, she is a technical assistant in fundamental project related to improving efficiency of silicon solar cell. She is good at TCAD simulation and programming in visual basic. She is the author of more than six articles. Her research interests include TCAD simulation, programming, metal oxides, heterojunctions, perovskites, and solar cells.